Research Square

Preprints are preliminary reports that have not undergone peer review.
They should not be considered conclusive, used to inform clinical practice,
or referenced by the media as validated information.

Potential flood risk under climate change: a local assessment in the absence of damage data

Alexander Gelfan

hydrowpi@mail.ru

Lomonosov Moscow State University Faculty of Geography: Moskovskij gosudarstvennyj universitet imeni M V Lomonosova Geograficeskij fakul'tet https://orcid.org/0000-0003-3288-1933

Inna Krylenko

Lomonosov Moscow State University Faculty of Geography: Moskovskij gosudarstvennyj universitet imeni M V Lomonosova Geograficeskij fakul'tet

Andrey Kalugin

Water Problems Institute Russian Academy of Sciences: Institut vodnyh problem Rossijskoj akademii nauk

Natalia Frolova

Lomonosov Moscow State University Faculty of Geography: Moskovskij gosudarstvennyj universitet imeni M V Lomonosova Geograficeskij fakul'tet

Georgy Arutyunyan

Lomonosov Moscow State University Faculty of Geography: Moskovskij gosudarstvennyj universitet imeni M V Lomonosova Geograficeskij fakul'tet

Research Article

Keywords: climate change, flood risk, local scale, EAD-model, lack of flood damage data, hydrodynamic model

Posted Date: November 6th, 2026

DOI: https://doi.org/10.21203/rs.3.rs-11368035/v1

License: This work is licensed under a Creative Commons Attribution 4.0 International License.
Read Full License

Potential flood risk under climate change: a local assessment in the absence of damage data

Abstract

A method is proposed for assessing flood risk changes for a local river reach under projected climate change scenarios. Such assessments are hampered by a lack of flood damage data, which makes it impossible to use traditional approaches based on damage-flow relationships derived from actual floodplain inundation. Typically, information regarding future floodplain development, essential for climate change impact studies of flood risk, is also unavailable. For a local reach of the Lena River near Yakutsk, we developed a method to assess potential risk within the flood zone. It is based on the Expected Annual Damage (EAD) model and, in the absence of actual damage data, utilizes a set of indices summarizing the impact of flow on structural damage. The traditional EAD model was modified to account for the combined effects of flow depth and velocity, simulated for the river floodplain section using a high-resolution two-dimensional hydrodynamic model. Annual peak flow changes at the inlet of the river section were calculated using a regional hydrological model driven by data from GCMs ensemble. It was found that, even under the low-emissions SSP1-2.6 scenario, potential risk could increase by 23–73%, depending on the level of structural damage. Under the SSP5-8.5 scenario, the risk of catastrophic structural damage would rise by 70%, while minor damage risk would more than triple. The proposed approach can provide insight into the impact of climate change on potential flood risk at a local site in the absence of the damage data required for traditional risk assessment methods.

Keywords: climate change, flood risk, local scale, EAD-model, lack of flood damage data, hydrodynamic model

1 Introduction

Globally, floods – fluvial, pluvial, and coastal – are the most dangerous natural disasters in terms of occurrence and the number of affected people, and the second in terms of economic damage (Centre…, 2026). In recent decades, from 1990 to 2022, hazardous floods occurred in 168 countries (86% of the current number of countries), affecting more than 3.2 billion people (40% of the current world population), resulting in more than 218,000 deaths and economic losses exceeding US$1.3 trillion (Liu, 2024). Early warning and flood mitigation methods are built on the risk management paradigm, within which flood risk is considered as a combination of the probability of occurrence of a hazardous phenomenon (hazard) and its negative consequences in terms of socio-economic damage (Merz et al., 2010). The latter, if the hazardous event occurs, depends on exposure (i.e., population density, the development and value of the infrastructure,

socioeconomic assets, and other exposed elements located in the potential flood zone) and vulnerability, i.e., the susceptibility of these exposed elements to the negative impacts of water flow. Managing risk through its components, hazard, exposure, and vulnerability, is a central paradigm not only in the problem of flood protection, but also in ensuring water security in general: "water security is about managing water risk" (OECD, p.13).

Fluvial floods are the most destructive globally and for continental regions of the world. Previous studies have indicated that the risk of major river floods is increasing globally (Caretta et al., 2022; Gudmundsson et al., 2026) and will increase in the near future (Dottori et al., 2018; Rogers et al., 2025). At the same time, there is a difference in the magnitude and even sign of the changes in flood risk between individual countries and regions of the world, which reflects the direction and significance of spatial changes in the individual risk components: hazard, exposure, and vulnerability (Hirabayashi et al., 2013; Tanoue et al., 2016). The latter depend, in turn, on socio-economic and institutional characteristics (level of GDP, political and social conditions, rates of economic development and settlement of flooded areas, availability and effectiveness of flood mitigation measures, availability and development of the insurance system, inflation rates, etc.) (Scussolini et al., 2016; Tanoue et al., 2016; Teklesadic et al., 2017; Gelfan, 2023; Sauer et al., 2024; Zhang et al., 2025; Devadas et al., 2025), as well as the specifics of regional climate change, primarily precipitation and air temperature, and hydrological processes (see the recent IPCC report (Seneviratne et al., 2021; Caretta et al., 2022) and references herein). The relative contributions of socioeconomic and climatic factors to the observed and projected increases in riverine flood risk also vary significantly across land areas, with some publications assessing the latter as more significant (Davenport et al., 2021; Gudmundsson et al., 2021). However, due to the multifactorial nature of flood risk, trends in its change and their attribution to climate change contain significant uncertainty (Meresa et al., 2021).

The studies, such as those listed above, show national or regional flood risk pictures, which are significant for the affected large-scale territories, but in reality, all flood impacts are felt locally, depend on local conditions and require local risk-based decisions. Large-scale assessments of economic and social risk rarely use detailed data on the topography of flooded areas and do not adequately take into account local features affecting flooding (Bates et al., 2021), which prevents these assessments from being transferred to the local level (the only example known to us of the use of such data at a national scale has been recently described by Paulik et al. (2026).

To effectively prepare for disasters and prioritize mitigation strategies at the local level, sound assessments of flood risk and its potential transformations under climate change are paramount. The foundations of the modern concept of risk were first set out in the classical decision theory (Wald, 1950), in which risk is defined as the mathematical expectation of losses

(damages). Owing to its fundamental basis, this rigorous concept has long been widely used to assess flood risk within the framework of the so-called flood damage models (USACE, 1994; Loucks et al., 2005; Merz et al., 2010; Verkade and Werner, 2011; Winsemius et al., 2013; Garrick and Hall, 2014; Montanari et al., 2024).

One of the effective, simple, and theoretically sound flood damage models is the hydroeconomic Expected Annual Damage model (EAD-model) (White, 1964), which links the flood frequency distribution through flood stage as an indicator of inundation depth to flood damage. Experience in using the EAD-model is represented by an extensive bibliography (see the recent review by Romali et al., 2025).

The EAD-model is a single-variable damage model (Molinari et al., 2020) and takes into account the water stage as a damage influencing parameter. The latter does not always explain flood damage. In fact, depending on the type of the flood-exposed objects and the characteristics of the flood, damage can be caused by many different processes, which in turn depend on various variables such as flow velocity, duration of the inundation, water depth rise rate, contamination of flood water, etc. (Lazzarin et al., 2022; Maranzoni et al., 2023). For example, the relationship between flow velocity and direct monetary damage from floods has been demonstrated for various destruction processes, such as physical damage to roads and buildings, vehicles, etc. (see, e.g., Kreibich et al., 2009; Garotte et al. 2016; Martínez-Gomariz et al., 2018; Lazzarin et al., 2022). It is widely accepted that the higher the flow velocity, the greater the likelihood of heavy structural damage to residential buildings, and the damage increases nonlinearly with increasing velocity (Soetanto and Proverbs, 2004; Kreibich et al., 2009). Schwarz and Maiwald (2008) studied the effect of modelled flow velocity on building damage using damage data collected from several floods in Germany. Comprehensive analysis of the influences of flow velocity, water depth and their combinations on various types of structural damage was carried out by Kreibich et al. (2009) for residential areas affected by the Elbe River flood in Germany in 2002. Flow velocity as a factor in catastrophic damage was analyzed using data on the consequences of the 2021 flood in Germany by Pažourková et al. (2022). Pistrika and Jonkman (2009), De Moel and Aerts (2011) showed that taking into account flow velocity along with inundation depth allows for more accurate estimation of flood damage.

The factors other than water stage are rarely taken into account in flood damage models as shown in many reviews (Merz et al., 2010; Molinari et al., 2020; Lazzarin et al., 2022; Romali et al., 2025), which may reduce the reliability of flood hazard and, as a consequence, flood risk assessment (Maranzoni et al., 2023). With the advent of satellite data on the dynamics of flood zones and high-resolution topographic data in recent decades, the development of computing resources and 2-D hydrodynamic models that allow the dynamics of depth fields, velocities and

flow directions to be described with high spatial resolution, the set of data that can be used for risk assessment has significantly expanded. At the same time, we know very few studies which have implemented flooding parameters other than water stage into the EAD-model. For example, using a 2-D hydrodynamic model based on LIDAR 1 m-topography, Garotte et al. (2016) simulated flow characteristics of the flooded area located in the floodplain of the Cega River (Italy) and linked them with stage–damage functions developed for exposed elements of urban-type categories. Lazzarin et al. (2022), although without the use of hydrodynamic simulation data, proposed an elegant method allowing for assessment of flood hazard based on non-dimensional physically meaningful parameter combining flow depth and velocity and directly associated with damaging potential for specific categories of objects. A comprehensive approach, combining a detailed hydrodynamic model and a flood damage analysis system based on the EAD-model, made it possible to assess the structural economic risk for the entire territory of New Zealand (Paulik et al., 2026).

Flood risk assessments under projected climate change are typically undertaken for large regions (see references above), where advanced 2-D hydrodynamic models are difficult to use. There are few examples of such assessments using the EAD model. Löschner et al. (2017) analyzed the impact of climate change and urban development in Austrian municipalities on future flood risk estimated by the EAD-model. The authors demonstrated that climate change and urban development significantly increase the potential flood risk. Here, floodplain topography and development type are key factors in determining the relative contribution of these drivers. Vidmar et al. (2025) used a 2-D hydrodynamic model to assess the impact of climate change on flood risk in the lower Vipava River (Slovenia). Using the EAD-model, the authors demonstrated a nonlinear increase in risk with increasing flood hazard on the river: a 20% increase in flood peaks projected under the RCP8.5 scenario would lead to a 40% increase in the risk.

Given the identified research gaps, our study objective was to assess the transformation of local flood risk under the influence of projected climate change using a two-dimensional hydrodynamic model and a modified EAD-model that takes into account not only flow depth but also flow velocity as influencing parameters. To achieve this objective, we sought answers to two poorly understood research questions that motivated our study. Firstly, how can additional influencing parameters be included in the EAD modelling framework to improve its performance? Secondly, how can the modified EAD model be coupled with an advanced 2D hydrodynamic model to assess local-scale flood risk under modern climate conditions and project it into the future?

In our study, we consider flood-induced damage to the structure of buildings, classified as a part of so-called structural damage (Schwarz and Maiwald, 2008; Kreibich et al., 2009; Garotte

et al. 2016; Martínez-Gomariz et al., 2018; Marvi, 2020; Pažourková et al., 2022). The key limiting factor in constructing a structural damage function for the EAD-model is the availability of detailed information on the types of buildings, their distribution over the area, occupancy type, construction material, repair and replacement cost, depreciation, etc. (Marvi, 2020). These data are high-dimensional, very expensive in terms of money, time and effort of their acquisition, and, as a result, they are not readily available in most countries (Rrokaj et al., 2025) including Russia. A particular data deficit is evident in the developed regions of northern Eurasia. To overcome this fundamental limitation, we proposed a method for determining potential structural damage and assessing local risk in the absence of detailed data. An attempt to develop such a method to achieve the above-mentioned goal is the third research issue posed in our study.

2 Case Study

The Lena River, one of the world's largest rivers, flows through Eastern Siberia into the Arctic Ocean. The 75-km section under consideration is located in the river's middle reach, near the city of Yakutsk, which has a population of 340,000. The inlet of this section is a streamflow and water-stage monitoring gauge located near the village of Tabaga (61°51′N, 129°35′ E) (Fig. 1). The drainage basin area at the gauge is 897,000 km². The climate is extremely continental: winters are cold, with temperatures dropping to –50°C or lower, while summers are hot. The majority of the drainage basin lies within the taiga zone, underlain by continuous or discontinuous permafrost.

In addition to the Tabaga gauge, there are two other measurement points within the section under consideration: a water-stage gauging station in the city of Yakutsk (in the middle part of the section) and the Kangalassy gauge at the downstream outlet (Fig. 1). The whole river section is characterized by numerous branches; the width of the main Lena channel here is 3.5–4 km, the floodplain width is 6–7 km, and the floodplain elevation reaches 10 m above the low-water level.

Fig. 1 The case study: the Lena River basin upstream of the Tabaga gauge (1) and the flood-prone river reach (2)

The water level regime of the Lena River near Yakutsk is characterized by a pronounced rise during the spring flood (including due to ice jams), significant and abrupt rises during summer-autumn floods, and relatively low, stable levels during the cold season. Ice jams lasting from one to five days occur in the Yakutsk area on average every one to two years–predominantly in sections where the river channel branches. The maximum water discharge was recorded on May 24, 1966 (50,900 m³/s); in the last two decades, values close to the record discharge were observed on June 11, 2006, and May 20, 2010 (49,600 m³/s and 47,000 m³/s, respectively). Overall, a statistically

significant increase in both mean and annual peak flow has been found (e.g. Tananaev et al., 2016); a trend that has become particularly apparent since the beginning of the 21st century.

3 Models, Data, and Experiment Design

3.1 Models

3.1.1 Regional Hydrological Model

The model of the Lena River basin (with the outlet at the Tabaga gauge) was developed based on the regional hydrological model ECOMAG (Motovilov et al., 1999). This model has been successfully applied for many years to describe hydrological processes and simulate river flow characteristics across catchments ranging from tens to millions of square kilometers in diverse climatic and physiographic conditions, including the Arctic region (Gelfan et al., 2017; Lisina et al., 2025, Razarenova, Krylenko, 2026). A description of the ECOMAG-based Lena River model and the results of evaluation of the model forced by the GSWP3-W5E5 reanalysis dataset were provided by Gelfan et al. (2023). Here, we assessed the suitability of that model for reproducing peak discharge (using the same reanalysis data) to serve as an upper boundary condition for the hydrodynamic model (Subsection 3.1.2). Additionally, the ESMs ensemble simulations (Subsection 3.2.1) were used to force the hydrological model, enabling an assessment of peak flow anomalies at the end of the 21st century relative to the historical period.

3.1.2 Hydrodynamic Model

For hydrodynamic modeling, the STREAM-2D software package was employed (Belikov et al., 2015; Aleksyuk, Belikov, 2019). It is based on the numerical solution of the two-dimensional Saint-Venant equations under the shallow-water approximation and utilizes hybrid unstructured computational grids and proprietary terrain interpolation algorithms (Belikov, Semenov, 2000). The model is equipped with an ice module that enables the simulation of flow dynamics in the presence of an ice cover. The modeled area, 75 km of the Lena river reach near Yakutsk, was discretized using detailed topographic and bathymetric data with a spatial resolution of 15–30 m for river channels and 100–300 m for the floodplain. For the study area, the model was successfully verified earlier with the use of multi-year discharge and water level observations (Golovlyov et al., 2019; Krylenko et al., 2024), satellite imagery of flooded areas (Kornilova et al., 2018), and satellite altimetry data, including during ice-cover periods (Zakharova et al., 2025), and was applied to simulate floods characteristics changes under CMIP5 projections (Krylenko, 2023).

3.1.3 Intensity-based Expected Annual Damage model

In addition to the hydrostatic action of the flow, proportional to its depth, one of the key mechanisms of structural flood damage is the hydrodynamic action of the flow (Kelman and Spence, 2004). We described the action by the intensity indicator determined as the product of the hydrodynamic pressure, proportional to the square of the flow velocity, and flow depth:

$$I = ph = 0.5\rho_W v^2 h, \quad (1)$$

where I is the intensity indicator [kg/s^2]; p is the hydrodynamic pressure [Pa]; h is the flow depth [m]; v is the flow velocity [m/s]; ρ_W is the water density [kg/m^3].

Formula (1) was used, for example, by Agafonova et al. (2017) and Kidyaeva et al. (2017) as the indicator of damage caused by ice-jam and glacial lake outburst floods, respectively. In the modified, intensity-based EAD model (hereafter referred to as the i_EAD model) that we propose and describe below, the flow intensity (1) is considered to be the parameter that influences damage. (Note that in a number of publications, e.g., Kreibich et al., 2009; Pažourková et al., 2022, the flow intensity indicator is calculated as the product of v and h).

Let Q be the annual peak discharge (APD) that causes flooding of the floodplain in a local section of the river valley. It is assumed that for the i-th mesh cell of the floodplain hydrodynamics model, the discharge Q is functionally related to the average flow intensity over the cell area as $Q = g_i(I_i)$, i=1, 2,…,N, where N is the number of the model cells. If the damage function for the i -th cell is determined as $D_i = D_i(I_i)$, then, there is an unambiguous discharge-damage relationship $D_Q = \sum_{i=1}^{N} D_i$, i.e. the total damage from flooding of the floodplain at a given boundary (inlet) flow rate Q is the sum of the damages for all cells. The following derivation of formulas for estimating the mathematical expectation of damage is based on the idea of the original model EAD-model (USACE, 1994; Verkade and Werner, 2011; Rosbjerg, 2024).

Let $F_Q(q) = P\{Q \le q\}$ be the cumulative distribution function (CDF) for the APD, $f_Q(q) = dF_Q(q)/dq$ the corresponding probability density function, and $F_Q^*(q) = P\{Q > q\} = 1 - F_Q(q)$ the exceedance probability function (survival function). Accordingly, flood risk defined as an expected annual damage (EAD), i.e. an expectation of the function D_Q of random variable $Q > 0$, is determined as:

$$RISK = EAD = \int_0^{\infty} D_Q(q) f_Q(q) dq = \quad (2)$$

$$= \int_0^1 D_p(p_Q) dp_Q \quad (3)$$

where $D_p(p_Q)$ is the damage caused by the discharge of the exceedance probability equal to p_Q or the damage caused by a flood event of the return period of p_Q^{-1} years.

Let us repeat that formulas (2), (3) are similar to the corresponding formulas used in the original model, but differ in the choice of the influencing (flooding) parameter and the flooding parameter-to-damage transition.

When damage data are insufficient to specify a continuous function $D_i = D_i(I_i)$, a stepwise flood damage function can be used (Rosbjerg, 2024). In this case, the damage is specified in the format of indices corresponding to a given range of intensities, and the integral in formula (3) is replaced by the sum:

$$EAD = \sum_{k=1}^{n} D_p(p_k)\, p_k \qquad (4)$$

where n is the number of intervals into which the segment [0;1] is divided in accordance with the number of intervals of the flood damage function.

3.2 Data

3.2.1 Climate Data

For the historical period, the ECOMAG hydrological model was forced using W5E5 v2.0 meteorological reanalysis data (a 0.5° latitude-longitude grid); this dataset covers the entire globe with a spatial resolution of 0.5° and a daily time step (Lange et al., 2021). The W5E5 dataset was prepared within phase 3b of the Inter-Sectoral Impact Model Intercomparison Project (ISIMIP3b) to correct systematic biases in the input climate data used for assessing climate change impacts. The data sources for W5E5 included: data derived by applying the WATCH Forcing Data methodology (version 2.0) to ERA5 data (WFDE5; Cucchi et al., 2020); ERA5 reanalysis data (Hersbach et al., 2020); and precipitation data from the Global Precipitation Climatology Project version 2.3 dataset (Adler et al., 2003). W5E5 reanalysis data were used to verify the hydrological model of the studied part of the Lena River basin.

For the historical period (1979-2010) and the final 30-year period of the 21st century (2070-2099), climate data from five Earth system models (GFDL-ESM4, IPSL-CM6A-LR, MPI-ESM1-2-HR, MRI-ESM2-0, UKESM1-0-LL) were also used in order to assess peak flow anomalies at the end of the 21st century relative to the historical period. The climate simulation data were downscaled and bias-adjusted against reanalysis data in accordance to the ISIMIP3 protocol; https://www.isimip.org/protocol/3/). The climate projection data corresponded to two SSP scenarios: SSP1-2.6, and SSP5-8.5. The SSP1-2.6 scenario assumes a sustainable development pathway with low radiative forcing. Atmospheric CO_2 concentration will peak around the mid-21st

century and then decline. The SSP5-8.5 scenario characterizes global development based on fossil fuels and the maximum level of greenhouse gas emissions. As the most pessimistic scenario, it implies a tripling of CO_2 emissions.

3.2.2 Land Surface Data

The Harmonized World Soil Database (HWSD – http://www.fao.org/soils-portal/data-hub/soil-maps-and-databases/harmonized-world-soil-database-v12) and the Global Land Cover Characterization (GLCC – https://www.usgs.gov/centers/eros/science/usgs-eros-archive-land-cover-products-global-land-cover-characterization-glcc) databases were used to set the land surface parameters for soil and landscape types in the ECOMAG hydrological model. Schematization of the catchments and river network was performed based on the HYDRO1k digital elevation model with a spatial resolution of 1 km (https://www.usgs.gov/centers/eros/science/usgs-eros-archive-digital-elevation-hydro1k).

For hydrodynamic modeling, we used detailed topography and bathymetry data described in (Golovlyov et al., 2019); for the floodplain additionally FABDEM topography data were acquired (Hawker, 2022).

3.2.3 Streamflow Data

Daily streamflow data from the Tabaga hydrological station, a part of the Roshydromet monitoring network, were used for the ECOMAG hydrological model evaluation for the 1979-2010 period.

3.3 Experiment Design

3.3.1 Evaluation of the hydrological model

The ECOMAG-based hydrological model (Gelfan et al., 2023) was forced by daily W5E5 reanalysis data (precipitation, air temperature, and moisture deficit) for 32 years, from Jan. 1, 1979 to Dec. 31, 2010. We applied three tests to evaluate the model. Firstly, the model was evaluated against the observed daily streamflow data. We followed the recommendations of Moriasi et al. (2015) regarding the threshold values of the model efficiency in terms of Nash-and-Sutcliffe efficiency (NSE) and Percent Bias (PBIAS) criteria. Secondly, we used a criterion like one proposed by Yilmaz et al. (2008), namely, %BiasFHV_{10}, that is, the percent bias in the flow-duration curve (FDC) high-segment flow volume for flows with exceedance probability lower than 10%:

$$\%\text{Bias}FHV_{10} = \frac{\sum_{h=1}^{H}(QS_h - QO_h)}{\sum_{h=1}^{H} QO_h} \times 100 \qquad (5)$$

where QO_h and QS_h are the FDC-ordinates derived from the observed and simulated daily streamflow data, respectively, $h = 1, 2, \ldots, H$, H is the number of the ordinates with the exceedance probabilities lower than 10%. We considered the model performance as "good" if $|\%\text{Bias}FHV_{10}|<5\%$.

Thirdly, we used two non-parametric statistical tests, namely, two-sample Kolmogorov-Smirnov test (KS-test) and Mann-Witney U-test, in order to compare statistical properties of the observed and simulated APD series over a 32-year period. Both KS-test and U-test allow us to recognize whether the independent series are covered by the same population and whether they are identically distributed. However, we used both tests because they are differently sensitive to distinct features of the compared data (Özçomak et al., 2013): the first one is more sensitive to changes in the shape and range of the distribution, while the second one is more sensitive to changes in the median and handles small samples better.

3.3.2 Assessment of annual peak discharge statistics in a future climate

Employing the verified ECOMAG model, the APD-series were simulated for the historical period 1979-2010, as well as for a 30-year period at the end of the 21st century using the ESMs climate projections under two IPCC scenarios: SSP1-2.6, a scenario of a sustainable, low-emissions climate pathway, and SSP5-8.5, a scenario of fossil-fueled development. Based on the simulation results, we determined the relative deviations (anomalies) of the mean and the coefficient of variation of APD at the end of the 21st century. The anomalies were averaged across the model ensemble for each scenario. By multiplying the averaged anomalies by the statistics of the historical APD-series simulated by the reanalysis data, we obtained the mean value and the coefficient of variation of APD for the end of the 21st century.

3.3.3 Flood risk assessment for current and future climates

The flood risk assessment algorithm based on the proposed i_EAD model is schematically presented in Fig. 2.

Fig. 2 Schematic representation of the i_EAD-model

One starts from the exceedance probability distribution $F_Q^*(q)$ of APD (top left panel). The I-Q curves (top right panel) link the discharge to flow intensity for each floodplain cell. The simulated intensity values correspond to local damages obtained from the damage D-I curves (bottom right panel). The sum of the local damages represents the total damage due to inundation of the floodplain, corresponding to the given APD. By relating the exceedance probabilities of each flood

discharge to the flow intensity and the resulting damage, one can establish a flood damage exceedance probability curve $D_p(p_Q)$ (bottom left panel). At the output of the procedure, the expected annual damage is calculated as the area under this curve (formula 3).

The data and dependencies for implementing the described risk assessment procedure were specified as follows.

A gamma distribution function was used to construct probability distributions of APD corresponding to historical and future climate conditions. The mean value and coefficient of variation of APD, calculated as described above (Subsection 3.3.2), were adopted as the parameters of the gamma distribution. As a result, we obtained three exceedance probability curves F_Q^* corresponding to the current climate and two future climate scenarios. Changes in these curves under different climatic conditions determine the transformation of flood risk in the local river section under consideration.

Flow intensities (1) were calculated using the STREAM-2D model for 11 values of input peak flow rates determined from the F_Q^*-curve and corresponding to exceedance probabilities of 0.1%, 1%, 5%, 10%, 25%, 50%, 75%, 90%, 95%, 99%, 99.9%. As a result, we obtained intensity values for each mesh cell, and from these data, we constructed a set of $I - Q$ curves, which are the dependences of local flow intensity on inlet discharge. Flow intensities were calculated for each of the three F_Q^*-curves corresponding to different climates, i.e., the flow intensity spatial distributions across flooded areas were calculated for 11 × 3 = 33 values of inlet discharge.

To define the $D_i = D_i(I_i)$ curves, we used an intensity-based method for earthquake damage analysis, adapted for flood damage assessment by Schwarz and Maiwald (2008). The authors identified five classes of structural damage, which are classified in order of increasing flood impact from "slight", with no visible structural damage to "very heavy," characterized by the collapse of buildings. In the Russian guide (EMERCOM, 2007), five similar classes of structural damage are distinguished according to flood intensity, calculated using formula (1) (Table 1).

We applied the above classification to assess the potential total damage in the floodplain. Potential damage is defined as the possible damage from floods of varying magnitudes under hypothetical floodplain development conditions (Smith, 1981). Total damage was assessed using the so-called threshold-type criterion (Pažourková et al., 2022) as follows. Based on the simulated values of flow intensity in each cell, we determined the structural damage class D_i and identified cells in the flooded area, for which $D_i \geq 4$; $D_i=3$; $D_i=2$. The sum of the areas A_i of the corresponding cells was used as an indicator of potential total damage for a given category. For example, for the category of greatest possible damage, $D_Q(heavy) = \sum_{i=1}^{N} k_i$, where $k_i = A_i$, if $D_i \geq 4$ and $k_i=0$ otherwise, N is the number of flooded cells of the modeling area. The D_Q values

for each category were calculated for each of the 11 values of the inlet discharge taken from the F_Q^*-curve, which was calculated either based on historical climate data or one of two future climate scenarios.

Based on the 11 values of potential structural damage determined in this way and their exceedance probabilities for a given climate and for the given damage category, the $D_p(p_Q)$ curve was constructed and the value of potential risk was calculated using formula (4).

Thus, the potential risk of structural damage of a given scale was assessed as the expected area (in km^2) of that part of the floodplain where, if it were fully built up, corresponding destruction could occur as a result of probable flooding in the given climatic conditions.

4. Results and Discussion

4.1 Evaluation of the hydrological model

Figure 3 compares actual and the ECOMAG-simulated daily streamflow series at the Tabaga gauge over a 32-year period, along with the flow duration curves and the annual peak flow probability curves. In Table S1, the metrics we used to assess the model's performance are presented.

Both the visual analysis of the graphs in Fig. S1 and the results presented in Table S1 show that the model reproduces well the water regime in the river under consideration, as well as the statistics of maximum annual discharges.

According to the recommendations of Moriasi et al. (2015), the model performance can be judged as "very good", since NSE>0.85 and $|PBIAS|$<5% for daily streamflow. The peak flow statistics (mean value and variance indicators) in the observed and calculated series also agree well with each other: differences between the statistics do not go beyond the 95% confidence intervals of their sampling error. Finally, both KS-test and U-test did not reject the null hypothesis at 5% significance level, i.e. the compared APD samples are identically distributed.

The obtained results allowed us to use the exceedance probability curves of the ECOMAG-simulated APDs for risk assessment and its transformation applying the i_EAD-model.

4.2 Flood risk assessments for current and future climate

The obtained results are presented below following the framework of the potential risk assessment procedure shown in Fig. 2 as: <exceedance probability of APD> => <intensity-discharge relationship> => <damage function> => <exceedance probability of damage> => <expected annual damage (RISK)>.

Table S2 shows the relative anomalies of the mean values and coefficients of variation of APD for the end of the 21st century compared to the corresponding statistics for the historical period. Both sets of statistics are determined from APD series simulated by climate models' data.

Figure 3 presents three probability distributions of APD, constructed using ensemble-averaged values of mean peak discharge and its coefficients of variation for the current climate and for two future climate change scenarios. Eleven Q-values corresponding to the exceedance probabilities listed above were taken from these three probability curves (Fig. 3) and assigned as input to the i_EAD model.

Fig. 3 Exceedance probabilities of annual peak discharge simulated under different climate

Under the SSP1-2.6 scenario, climate change can lead to a moderate effect on the probability distribution: the mean value of APD increased by 11% and the variance rose by 7% compared to the historical period, due to that APDs increased across the entire range of exceedance probabilities, especially noticeably for 0.1-1%. Overall, the calculated changes in exceedance probability curves under the given climate change scenario significantly exceed the sampling variability of the corresponding statistical metrics estimated from 32 years of data.

Climate change under the SSP5-8.5 scenario resulted in a 24-42% (34% on average) increase in APD for all exceedance probabilities, significantly exceeding their sample variability. Visible changes in discharges for low exceedance probabilities were found, which have the greatest impact on potential structural damage during flooding of the study area. For instance, the maximum discharge recorded during the observation period, 50,900 m^3/s on May 24, 1966, which, under the current climate, has an exceedance probability about 1%, can be exceeded with a probability of 50% under this severe scenario.

The next step in the risk assessment procedure (Fig. 2) is to construct curves relating flow intensity to the input peak discharge with a given exceedance probability for each grid cell. An example of such curves, constructed for several cells within a small and relatively homogeneous part of the floodplain, is shown in Fig. 4.

Fig. 4 $Q - I$ relationships for some closely located model cells on the floodplain

The differences between the curves calculated for different climates for a single cell are much less pronounced than the spatial differences between the curves calculated for different cells under the same climate. Variability in floodplain topography is thus a key factor in the variability of the flow's hydraulic properties and its impact on buildings, i.e., a much more significant factor

443 in potential structural damage than climate-induced changes in inlet peak flow; it is the conclusion,
444 which is consistent with the results of previous studies (see, for example, Löschner et al. (2017)).
445 It is important to note that floodplain topography influences not only the absolute values
446 of flow intensity for a given input discharge, but also the shape of the $Q - I$ relationships. As
447 Figure 4 shows, these relationships are not only nonlinear but may also be nonmonotonic, meaning
448 that for some cells, flow intensity may increase with decreasing input discharge, and vice versa.
449 This effect is due to the fact that, for certain combinations of cell topographic parameters, changes
450 in input discharge can lead to opposite changes in flow velocity and flow depth within a specific
451 cell. The sensitivity of flow intensity to changes in velocity is twice as high as to changes in depth
452 (this can be easily demonstrated by differentiating formula (1)). In other words, in certain areas of
453 the floodplain, the hydrodynamic impact of the flow on buildings and the resulting structural
454 damage may increase with decreasing inlet discharge and flow depth. Therefore, using flow depth
455 as the sole damage influencing parameter may lead to an incorrect assessment of the direction of
456 changes in structural damage with changes in inlet discharge. This result confirms the findings of
457 many previous studies mentioned above that the consideration of water depth alone may be
458 insufficient in flood risk assessment (Kreibich et al., 2009; Pistrika and Jonkman, 2009; De Moel
459 and Aerts, 2011; Garotte et al., 2016; Martínez-Gomariz et al., 2018; Marvi, 2020; Pažourková et
460 al., 2022; Maranzoni et al., 2023 and others). Furthermore, this result highlights the importance of
461 hydrodynamic modeling of flow characteristics in the flood zone as a source of information
462 missing from streamflow measurements and as a tool for describing nonlinear hydrodynamic
463 effects of flow impacts.
464 Indicators of potential structural damage that depend on flow intensity also exhibit
465 significant spatial variability. These indicators, corresponding to inlet discharges with a given
466 probability, were determined for each of the 21,036 cells of the computational grid across the
467 floodplain. An example of the distribution of the damage indicators across the flood zone at a 1%
468 probability inlet flow rate, corresponding to the current climate and the most severe climate change
469 scenario, is shown in Fig. 5. It is evident that, with the same input flow rate, potential damage
470 indicators in different parts of the floodplain can vary from no visible damage to possible complete
471 destruction of buildings. Moreover, as expected, the spatial variability of the indicators is much
472 greater than their variability due to climate change, confirming the conclusion that topography
473 dominates the climate factor in risk assessment.
474
475 **Fig. 5** The damage indicators across the flood zone at a 1% probability inlet flow rate,
476 corresponding to the current climate (a) and the SSP5-8.5 climate change scenario (b)
477

Based on the data obtained, the total areas of the cells where damage indicators corresponded to a particular level were calculated. Figure 6 shows the probability distributions of the exposed areas, which were used to determine the EAD (risk) values.

Fig. 6 Exceedance probabilities of areas whose flooding would result in potential damage of varying levels under current and future climate conditions

The potential risk of structural damage defined in terms of the expected area of possible damage and calculated from the probability curves is presented in Table 2.

Even under the SSP1-2.6 low-emissions climate pathway scenario, the level of potential risk in all categories increases significantly (by 23-73%) compared to the historical period. However, as can be seen in Fig. 6, the increase associates primarily with low and moderate structural damage. The SSP5-8.5 scenario, which entails the intensive use of fossil fuels, could lead to an even sharper increase in potential structural damage compared to current levels – 70-345%, depending on the damage category. Again, the greatest relative increase occurred for the potential risk of moderate and low categories of damage, not for heavy and very heavy damage. At first glance, this is a somewhat unexpected result, given the minimal baseline (only 0.64 km^2) against which changes in catastrophic damage risk were compared. The analysis revealed that the most significant changes in risk occurred due to the expansion of the flooded area, i.e., the flooding of areas that remained unaffected by floods in the modern climate. In other words, the main factor driving risk change is the increase in flood exposure – spread of potential damage in floodplain areas not affected by floods in the modern climate. Increases in flow depth and velocity in areas currently and prospectively subject to flooding proved to be a less significant factor in rising risk. Furthermore, the nonlinear nature of risk change is noteworthy: a 24%-42% increase in peak discharges of varying probabilities under the SSP5-8.5 scenario resulted in 70%-345% changes in risk. The nonlinear increase in flood risk with rising flood magnitude is consistent with the findings of previously published studies (e.g., Löschner et al., 2017; Vidmar et al., 2025).

It is important to note two issues related to the proposed methodology.

The first issue is related to the choice of the flow intensity indicator in form (1) as the influencing parameter of the i_EAD model. On the one hand, water depth and flow velocity have recently become much more common variables for quantifying flood damage, both individually and in combination (Maranzoni et al., 2023). On the other hand, choosing the most reasonable combination for specific types of structural damage is a complex task that, in the absence of damage data, must be addressed by taking into account the results of similar studies for other, more data-rich regions. For example, Kreibich et al. (2009) used damage data for the August 2002 flood

in Germany to evaluate the correlation of damage with flow velocity v and depth h, as well as three combinations of these variables: $h + v^2/2g$ (specific energy head indicator), hv^2 (flow force indicator), and hv (intensity indicator). For the used data, the authors found that depth and energy head have occurred to be more correlated with the level of damage (Kreibich et al., 2009). Using detailed damage data from the later 2021 flood in Germany confirmed the significance of the specific energy head as an indicator of catastrophic structural damage (Pažourková et al., 2022). Furthermore, some studies show that water depth alone remains not infrequently the best predictor of damage for a particular building type (Thieken et al., 2005; Marvi, 2020) as it is assumed within the classical EAD-approach. Finally, other influencing parameters, not just depth and flow velocity, can significantly increase structural damage under certain conditions, such as duration of inundation, contamination, etc. (references to relevant studies are provided by Marvi, 2020). The diversity of results highlights the need for further research aimed at ranking flooding parameters for specific types of floodplain development. In the absence of these data, as well as information on the floodplain development, the use of generalized information on the relationship between flow intensity in form (1) and structural damage (Table 1) seems to be reasonable.

The second problem is closely related to the first one and concerns the choice of damage functions that relate the damage to the corresponding floodplain element at risk to the above influencing parameters. In accordance with the above-mentioned multiplicity of the parameters, the damage function is also multidimensional and assigning it in a reliable and compact form is challenging. Moreover, as noted above, information on damage is insufficient even in developed countries (Wen et al., 2022), and in the vast majority of countries it remains extremely scarce (Romali et al., 2025) or unavailable (Rrokaj et al., 2025). Russia is not an exception in this regard. This data scarcity hinders the implementation of the damage functions developed for data-richer regions (Rrokaj et al., 2025). Conducting research aimed at developing methods for transferring damage data to areas not provided with this information seems more than relevant. In the absence of damage data in the study area and methods for transferring data from other areas, the approach we have developed to assessing potential risk, based on generalized, averaged data, seems to us to be an acceptable compromise. It is important to emphasize that the described approach cannot be used for the tasks of operational flood mitigation, when management decisions require detailed information on the consequences of flooding. However, this approach may be in demand for assessing the impact of climate change on the potential risk of floods, given the uncertainty of the simulated hydrological and climate data, the lack, as a rule, of data on future development on the floodplain and, most importantly, the focus of the developed method on assessing the risk at a climatic time scale, i.e. the average risk over a long period.

5 Conclusion

The main results of our study can be summarized as follows:

1. A modification of the widely accepted Expected Annual Damage (EAD) model of flood risk – i_EAD model – is proposed. In addition to water stage (the sole damage-influencing parameter representing the hydrostatic effect of flooding), we introduce a composite parameter that also accounts for flow velocity as an indicator of the hydrodynamic action of the flow. On the basis of simulated data from the STREAM-2D hydrodynamic model of the floodplain and the regional hydrological ECOMAG model, a procedure is developed to transform the probability distribution of annual peak discharge at the inlet of the river reach into probability distributions of damage at various floodplain locations and, ultimately, to a flood risk assessment.

2. A method is proposed allowing one to estimate potential structural damage during floodplain inundation in the absence of actual damage data, which is a common situation for the vast majority of the world's regions. The method relies on generalized information regarding the impact of flow on buildings and is presented as a set of indices that reflect the level of potential damage based on flow intensity. As a result, potential structural risk, i.e. flood risk under hypothetical floodplain development, is calculated by the i_EAD model as the expected area of the floodplain portion where, assuming continuous development, damage of the corresponding magnitude could occur due to a probable flood.

3. The developed methodology driven by the hydrology-and-hydrodynamic simulation data is used to assess the changes in the potential structural risk of floodplain inundation along the Lena River (near the city of Yakutsk) under projected climate conditions for the end of the 21st century. The results indicate that even under the mildest scenario, the low-emissions SSP1-2.6 pathway, potential structural risk could increase significantly, by 23–73%, depending on the level of damage. Under the least favorable scenario (SSP5-8.5), the risk of catastrophic structural damage would rise by 70%, while the risk of minor damage would more than triple. Furthermore, the potential risk increases much faster than the annual peak discharge rises owing to climate change.

References

Adler RF, Huffman GJ, Chang A et al (2003) The version 2 global precipitation climatology project (GPCP) monthly precipitation analysis (1979-present). J Hydrometeorol 4:1147–1167.

Agafonova S, Frolova N, Krylenko I et al (2017) Dangerous ice phenomena on the lowland rivers of European russia. Nat Haz 88(S1):171–188. https://doi.org/10.1007/s11069-016-2580-x

Aleksyuk AI, Belikov VV (2019) The uniqueness of the exact solution of the Riemann problem for the shallow water equations with discontinuous bottom. J Comp Phys 390:232–248. https://doi.org/10.1016/j.jcp.2019.04.001

Bates PD, Quinn N, Sampson C et al (2021) Combined modeling of US fluvial, pluvial, and coastal flood hazard under current and future climates. Water Resour Res 57:e2020WR028673. https://doi.org/10.1029/2020WR028673

Belikov VV, Krylenko IN, Alabyan AM et al (2015) Two-dimensional hydrodynamic flood control for the populations of the Russian rivers. Proc IAHS 370:69–74. https://doi.org/10.5194/piahs-370-69-2015

Belikov VV, Semenov AYu (2000) Non-Sibsonian interpolation of arbitrary system of points in Euclidean space and adaptive isolines generation. Appl Numer Math 32(4):371–387.

Caretta MA, Mukherji A, Arfanuzzaman M et al (2022) Water. In: Climate change 2022: impacts, adaptation and vulnerability. In: Portner HO et al (eds) Contribution of working group II to the sixth assessment report of the intergovernmental panel on climate change. Cambridge Univ Press, Cambridge and NY:551–712. https://doi.org/10.1017/9781009325844.006

Centre for Research on the Epidemiology of Disasters (CRED) & United Nations Office for Disaster Risk Reduction (UNDRR) (2026). 2025 Disasters in numbers. https://files.emdat.be/reports/2025_EMDAT_report.pdf

Cucchi M, Weedon GP, Amici A et al (2020) WFDE5: bias-adjusted ERA5 reanalysis data for impact studies. Earth Syst Sci Data 12:2097–2120.

Davenport FV, Burke M, Diffenbaugh NS (2021) Contribution of historical precipitation change to US flood damages. Proc Nat Ac Sci 118(4):e2017524118. https://doi.org/10.1073/pnas.2017524118

De Moel H, Aerts JCJH (2011) Effect of uncertainty in land use, damage models and inundation depth on flood damage estimates. Nat Haz 58(1):407–425. https://doi.org/10.1007/s11069-010-9675-6

Devadas B, Paprotny D, Kreibich H et al (2025) Projecting future flood losses to company assets in Europe: The role of precautionary measures. Earth's Future 13:e2025EF006285. https://doi.org/10.1029/2025EF006285

Dottori F, Szewczyk W, Ciscar JC et al (2018) Increased human and economic losses from river flooding with anthropogenic warming. Nat Clim Change 8(9). https://doi.org/10.1038/s41558-018-0257-z

EMERCOM of Russia (2007) Methodological recommendations for determining the number of victims in emergency situations. No. 1-4-60-9-9. Moscow, EMERCOM.

Garrick D, Hall J (2014) Water security and society: risks, metrics, and pathways. Annual Review of Environ and Resour 39:611–639. https://doi.org/10.1146/annurev-environ-013012-093817

Garrote J, Alvarenga FM, Díez-Herrero A (2016) Quantification of flash flood economic risk using ultra-detailed stage–damage functions and 2-D hydraulic models. J Hydrol 541:611–625. https://doi.org/10.1016/j.jhydrol.2016.02.006

Gelfan A (2023) Climate change and threats to water security: a review. Water Resour 50(5):645–663. https://doi.org/10.1134/S0097807823600547

Gelfan A, Gustafsson D, Motovilov Yu et al (2017) Climate change impact on the water regime of two great Arctic rivers: modeling and uncertainty issues. Clim Change 141:499–515. https://doi.org/10.1007/s10584-016-1710-5

Gelfan A, Kalugin A, Krylenko I (2023) Detection, attribution, and specifying mechanisms of hydrological changes in geographically different river basins. Clim Change 176:122–142. https://doi.org/10.1007/s10584-023-03557-6

Golovlyov P, Kornilova E, Krylenko I et al (2019) Numerical modeling and forecast of channel changes on the river Lena near city Yakutsk. Proc IAHS 381:65–71. https://doi.org/10.5194/piahs-381-65-2019

Gudmundsson L, Boulange J, Do HX et al (2021) Globally observed trends in mean and extreme river flow attributed to climate change. Science 371(6534):1159–1162. https://doi.org/10.1126/science.aba3996

Gudmundsson L, Brunner MI, Döll P et al (2026) Past and future change in global river flows. Nat Rev Earth Environ 7:7–23. https://doi.org/10.1038/s43017-025-00745-z

Hawker LP, Uhe P, Paulo L et al (2022) A 30 m global map of elevation with forests and buildings removed. Environ Res Lett 17(2):024016. https://doi.org/10.1088/1748-9326/ac4d4f

Hersbach H, Bell B, Berrisford P et al (2020) The ERA5 global reanalysis. Q J Roy Meteor Soc 146(730):1999–2049. https://doi.org/10.1002/qj. 3803

Hirabayashi Y, Mahendran R, Koirala S et al (2013) Global flood risk under climate changeю Nat Clim Change 3:816–821. https://doi.org/10.1038/nclimate1911

Kelman I, Spence R (2004) An overview of flood actions on buildings. Eng Geol 73:297–309.

Kidyaeva V, Chernomorets S, Krylenko I et al (2017) Modeling potential scenarios of the Tangjiashan lake outburst and risk assessment in the downstream valley. Frontiers of Earth Sci in China 11(3):579–591. https://doi.org/10.1007/s11707-017-0640-5

Kornilova E, Krylenko I, Golovlev P et al (2018) Verification of a 2D hydrodynamic model of the Lena River near Yakutsk using multi-temporal satellite imagery. Modern Problems of Remote Sensing of the Earth from Space 15(5):169–178. https://doi.org/10.21046/2070-7401-2018-15-5-169-178 (In Russian)

Kreibich H, Piroth K, Seifert I et al (2009) Is flow velocity a significant parameter in flood damage modelling? Nat Haz and Earth Syst Sci 9(5):1679–1692. https://doi.org/10.5194/nhess-9-1679-2009

Krylenko IN (2023) Evaluating inundation characteristics under climate changes. Wat Resour 50(4):577–582.

Krylenko IN, Pavlyukevich ED, Zavadskii AS et al (2024) Modelling of potential impact of climate change on water regime and channel processes in the river Lena near city Yakutsk: possibilities and limitations. Geography, Environment, Sustainability 17(4):112–120.

Lange S, Menz C, Gleixner S et al (2021) WFDE5 over land merged with ERA5 over the ocean (W5E5 v2.0). https://doi.org/10.48364/ISIMIP.342217

Lazzarin T, Viero D, Molinari D et al (2022) Flood damage functions based on a single physics- and data-based impact parameter that jointly accounts for water depth and velocity. J of Hydrology 607:127485. https://doi.org/10.1016/j.jhydrol.2022.127485

Lisina AA, Frolova NL, Kalugin AS et al (2025) Assessment of the Kolyma river hydrological regime dynamics in the 21st century based on runoff formation model. Geography, Environment, Sustainability 18(1):23–34. https://doi.org/10.24057/2071-9388-2025-3482

Liu Q, Du M, Wang Y et al (2024) Global, regional and national trends and impacts of natural floods, 1990–2022. Bull WHO 102:410–420. https://doi.org/10.2471/BLT.23.290243

Löschner L, Herrnegger M, Apperl B et al (2017) Flood risk, climate change and settlement development: a micro-scale assessment of Austrian municipalities. Reg Environ Change 17:311–322. https://doi.org/10.1007/s10113-016-1009-0

Loucks D, Van Beek E, Stedinger J et al (2005) Water resources systems planning and management: an introduction to methods, models and applications. UNESCO, Paris.

Maranzoni A, D'Oria M, Rizzo C (2023) Quantitative flood hazard assessment methods: A review. J of Flood Risk Manag 16(1):e12855. https://doi.org/10.1111/jfr3.12855

Martínez-Gomariz E, Gómez M, Russo B et al (2018) Stability criteria for flooded vehicles: A state-of-the-art review. J of Flood Risk Manag 11:S817–S826. https://doi.org/10.1111/jfr3.12262

Marvi TM (2020) A review of flood damage analysis for a building structure and contents. Nat Haz 102. https://doi.org/10.1007/s11069-020-03941-w

Meresa H, Murphy C, Fealy R et al (2021) Uncertainties and their interaction in flood hazard assessment with climate change. Hydrol Earth Syst Sci 25:5237–5257. https://doi.org/10.5194/hess-25-5237-2021

Merz B, Kreibich H, Schwarze R et al (2010) Review article "Assessment of economic flood damage". Nat Haz Earth Syst Sci 10:1697–1724. https://doi.org/10.5194/nhess-10-1697-2010

Molinari D, Scorzini AR, Arrighi C et al (2020) Are flood damage models converging to "reality"? Lessons learnt from a blind test. Nat Haz Earth Syst Sci 20:2997–3017. https://doi.org/10.5194/nhess-20-2997-2020

Montanari A, Merz B, Blöschl G (2024) HESS Opinions: The sword of Damocles of the impossible flood. Hydrol Earth Syst Sci 28:2603–2615. https://doi.org/10.5194/hess-28-2603-2024

Moriasi DN, Zeckoski RW, Arnold JG et al (2015) Models: performance measures and evaluation criteria. Trans ASABE 58(6):1763–1785. https://doi.org/10.13031/trans.58.10715

Motovilov YG, Gottschalk L, Engeland K et al (1999) Validation of a distributed hydrologicalmodel against spatial observations. Agric For Meteorol 98-99:257–277. https://doi.org/10.1016/S0168-1923(99)00102-1

OECD (2013) Water security for better lives. OECD Publishing. http://dx.doi.org/10.1787/9789264202405-en

693 Özçomak MS, Kartal M, Senger Ö et al (2013) Comparison of the powers of the Kolmogorov-Smirnov
694 two-sample test and the Mann-Whitney test for different kurtosis and skewness coefficients using
695 the Monte Carlo simulation method. J Statistical and Econometric Methods 2(4):81–98.
696 Paulik R, Hosse L, Pelmard J et al (2026) Evaluating New Zealand's building risk to fluvial and pluvial
697 flooding. Discov. Hazards 2(2). https://doi.org/10.1007/s44475-026-00010-x
698 Pažourková E, Salaj M, Wong Montoya RE (2022) Incorporation of flow velocity in flood damage
699 estimation: Ahr River Valley 2021 study, Germany. In Urban water systems & Floods IV, WIT
700 Press 208:15–26. https://doi.org/10.2495/FRIAR220021
701 Pistrika AK, Jonkman SN (2009) Damage to residential buildings due to flooding of New Orleans after
702 hurricane Katrina. Nat Haz 54(2):413–434. https://doi.org/10.1007/s11069-009-9476-y
703 Razarenova AD, Krylenko IN (2025) Runoff modeling for the Tom' River basin in a changing climate.
704 Russ Meteorol Hydrol 50:996–1005. https://doi.org/10.3103/S1068373925110081
705 Rogers JS, Maneta MP, Sain SR et al (2025) The role of climate and population change in global flood
706 exposure and vulnerability. Nat Commun 16:1287. https://doi.org/10.1038/s41467-025-56654-8
707 Romali NS, Sulong S, Kawasaki AA (2025) Systematic Review of flood damage assessment: Insight for
708 the data-Scarce regions. Water Resour Manage 39:4707–4734. https://doi.org/10.1007/s11269-
709 025-04265-9
710 Rosbjerg D (2024) Estimation of expected annual damage. Proc IAHS 385:25–29.
711 https://doi.org/10.5194/piahs-385-25-2024
712 Rrokaj S, Molinari D, Idarraga C et al (2025) Flood risk assessment and participative process in the data-
713 scarce Metuge district of Mozambique: An exportable approach. Int J of Disaster Risk Reduction
714 116:105163. https://doi.org/10.1016/j.ijdrr.2024.105163
715 Sauer IJ, Mester B, Frieler K et al (2024) Limited progress in global reduction of vulnerability to flood
716 impacts over the past two decades. Commun Earth Environ 5:239. https://doi.org/10.1038/s43247-
717 024-01401-y
718 Schwarz J, Maiwald H (2008) Damage and loss prediction model based on the vulnerability of building
719 types. In: 4th international symposium on flood defence, Canada:6–8.
720 Scussolini P, Aerts JCJH, Jongman B et al (2016) FLOPROS: an evolving global database of flood
721 protection standards. Nat Haz Earth Syst Sci 16(5):1049–1061. https://doi.org/10.5194/nhess-16-
722 1049-2016
723 Seneviratne SI, Zhang X, Adnan M et al (2021) Weather and climate extreme events in a changing climate.
724 In: Climate Change 2021: The physical science basis. Contribution of working group I to the Sixth
725 assessment report of the Intergovernmental Panel on Climate Change. Cambridge Univ. Press,
726 Cambridge and New York.
727 Smith DI (1981) Actual and potential flood damage: a case study for urban Lismore. NSW, Australia,
728 Applied Geography 1(1):31–39.
729 Soetanto R, Proverbs DG (2004) Impact of flood characteristics on damage caused to UK domestic
730 properties: the perceptions of building surveyors. Structural Survey 22(2):95–104.

731 Tananaev NI, Makarieva OM, Lebedeva LS (2016) Trends in annual and extreme flows in the Lena River
732 basin, Northern Eurasia. Geophys Res Lett 43:10764–10772.
733 https://doi.org/10.1002/2016GL070796
734 Tanoue M, Hirabayashi Y, Ikeuchi H (2016) Global-scale river flood vulnerability in the last 50 years. Sci
735 Rep 6:36021. https://doi.org/10.1038/srep36021
736 Teklesadik AD, Alemayehu T, van Griensven A et al (2017) Inter-model comparison of hydrological
737 impacts of climate change on the Upper Blue Nile basin using ensemble of hydrological models
738 and global climate models. Clim Change 141:517–532. https://doi.org/10.1007/s10584-017-1913-
739 4
740 Thieken AH, Müller M, Kreibich H et al (2005) Flood damage and influencing factors: New insights from
741 the August 2002 flood in German. Water Resour Res 41:W12430.
742 https://doi.org/10.1029/2005WR004177
743 USACE: Framework for estimating national economic benefits and other beneficial effects of flood
744 warning and preparedness systems (1994) Tech rep, US Army Corps of Engineers, Inst for Water
745 Resour, Virginia, USA.
746 Verkade JS, Werner MGF (2011) Estimating the benefits of single value and probability forecasting for
747 flood warning. Hydrol Earth Syst Sci 15:3751–3765. https://doi.org/10.5194/hess-15-3751-2011
748 Vidmar A, Ghebrebimichael FG, Rusjan S (2025) Climate change and the escalating cost of floods: new
749 insights from regional risk assessment perspective. Climate 13(11):223.
750 https://doi.org/10.3390/cli13110223
751 Wald A (1950) Statistical decision functions. J Wiley & Sons.
752 Wen X, Ferreira AMA, Rae LM et al (2022) A comprehensive methodology for evaluating the economic
753 impacts of floods: An application to Canada, Mexico, and the United States. Sustainability
754 14:14139. https://doi.org/10.3390/su142114139
755 White GF (1964) Choice of adjustment to floods. Research paper no. 93. Dep of Geogr, Univ of Chicago,
756 USA.
757 Winsemius HC, Van Beek LPH, Jongman B et al (2013) A framework for global river flood risk
758 assessments. Hydrol Earth Syst Sci 17:1871–1892. https://doi.org/10.5194/hess-17-1871-2013
759 Yilmaz KK, Gupta HV, Wagener T et al (2008) A process-based diagnostic approach to model evaluation:
760 application to the NWS distributed hydrologic model. Water Resour Res 44:W09417.
761 https://doi.org/10.1029/2007WR006716
762 Zakharova EA, Krylenko IN, Golovlev PP et al (2025) Satellite altimetry over frozen rivers. Satellite
763 altimetry and hydrodynamic model reproduce the ice jam conditions. Adv in Space Res 77:4352–
764 4363. https://doi.org/10.1016/j.asr.2025.11.121
765 Zhang Q, Li C, Wen D et al (2025) Global South shows higher urban flood exposures than the Global North
766 under current and future scenarios. Commun Earth Environ 6:594. https://doi.org/10.1038/s43247-
767 025-02585-7

768 **Statements&Declarations**

Ethics approval and consent to participate

Not applicable

Consent for publication

All necessary consents for publication have been obtained.

Competing Interests

The authors have no relevant financial or non-financial interests to disclose.

Author contributions

Conceptualization: A.G., I.K., and N.F.

Methodology: A.G.

Simulation: I.K. and G.A.

Visualization: A.G., I.K., and A.K.

Validation: A.G., I.K., and A.K.

Writing (original draft): A.G.

Writing (review and editing): A.G., I.K., A.K., and N.F.

Funding

Not applicable

Availability of data and materials

Historical climate data W5E5v2.0 https://www.isimip.org/gettingstarted/input-data-bias-adjustment/details/114/

Climate projections https://protocol.isimip.org/#/ISIMIP3a/water_regional/31-forcing-data

The Harmonized World Soil Database (HWSD) http://www.fao.org/soils-portal/data-hub/soil-maps-and-databases/harmonized-world-soil-database-v12)

The Global Land Cover Characterization (GLCC – https://www.usgs.gov/centers/eros/science/usgs-eros-archive-land-cover-products-global-land-cover-characterization-glcc)

The used daily streamflow data at the Tabaga hydrological station are not publicly available under applicable legislation

Table 1 Classes of structural damage according to flood intensity

Class of intensity	Intensity range ($kg \cdot s^{-2}$)	Structural Damage	Comments
1	< 62.5	No	Penetration and pollution only
2	62.5 – 1000	Low	Slight cracks in load-bearing elements broken doors and windows, contamination replacement of extension elements
3	1000 – 4500	Moderate	Deformations in load-bearing walls and slabs, settlement replacement of non-load bearing elements

4	4500 – 44600	Heavy	Structural collapse of load-bearing walls
5	> 44600	Very Heavy	Collapse of the building or of major parts of the building

797

798

799 **Table 2** Expected area (km^2) of potential structural damage of varying magnitudes in different climatic
800 conditions

Structural damage (category)	Description	Historical climate	Future climate	
			SSP1-2.6	SSP5-8.5
Low (2)	Minor structural damage to load-bearing elements and violations of integrity	63.06	109.37	210.92
Moderate (3)	Deformation of load-bearing walls and destruction of non-load-bearing elements	2.17	3.58	9.67
Heavy and very heavy (4,5)	Collapse of load-bearing walls or entire buildings	0.64	0.79	1.10

801

802

803

Figures

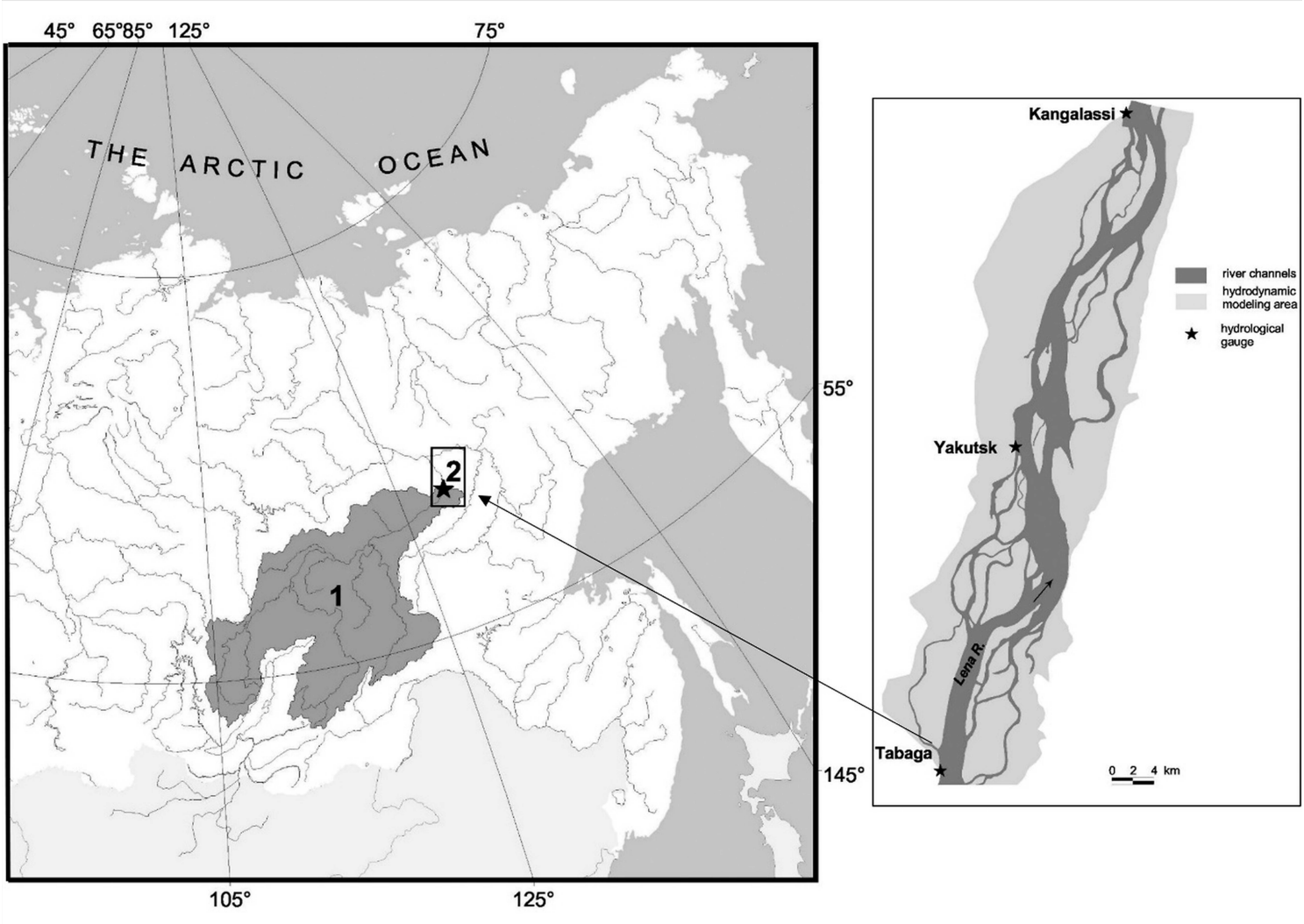


Figure 1

The case study: the Lena River basin upstream of the Tabaga gauge (1) and the flood-prone river reach (2)

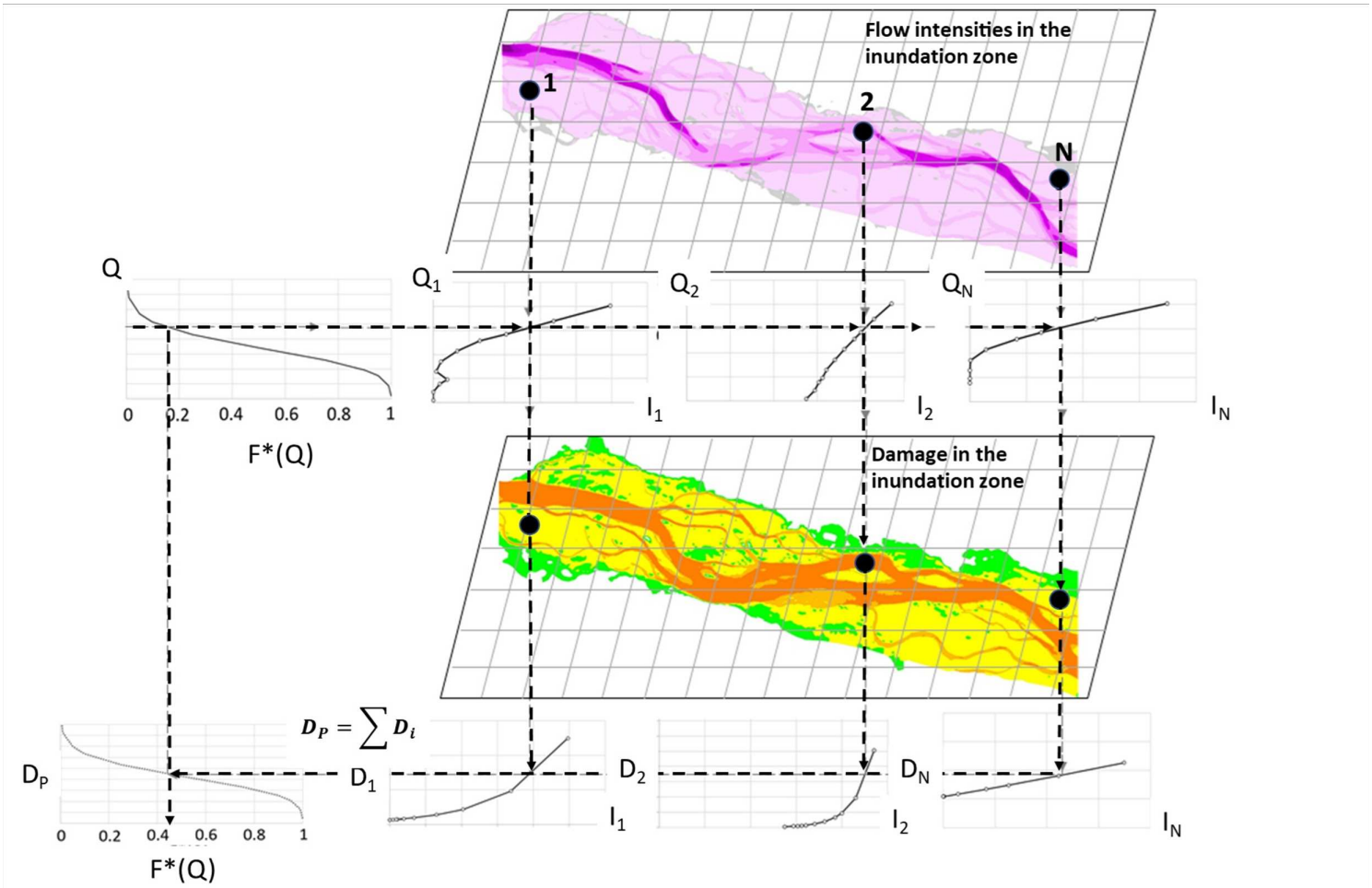


Figure 2

Schematic representation of the i_EAD-model

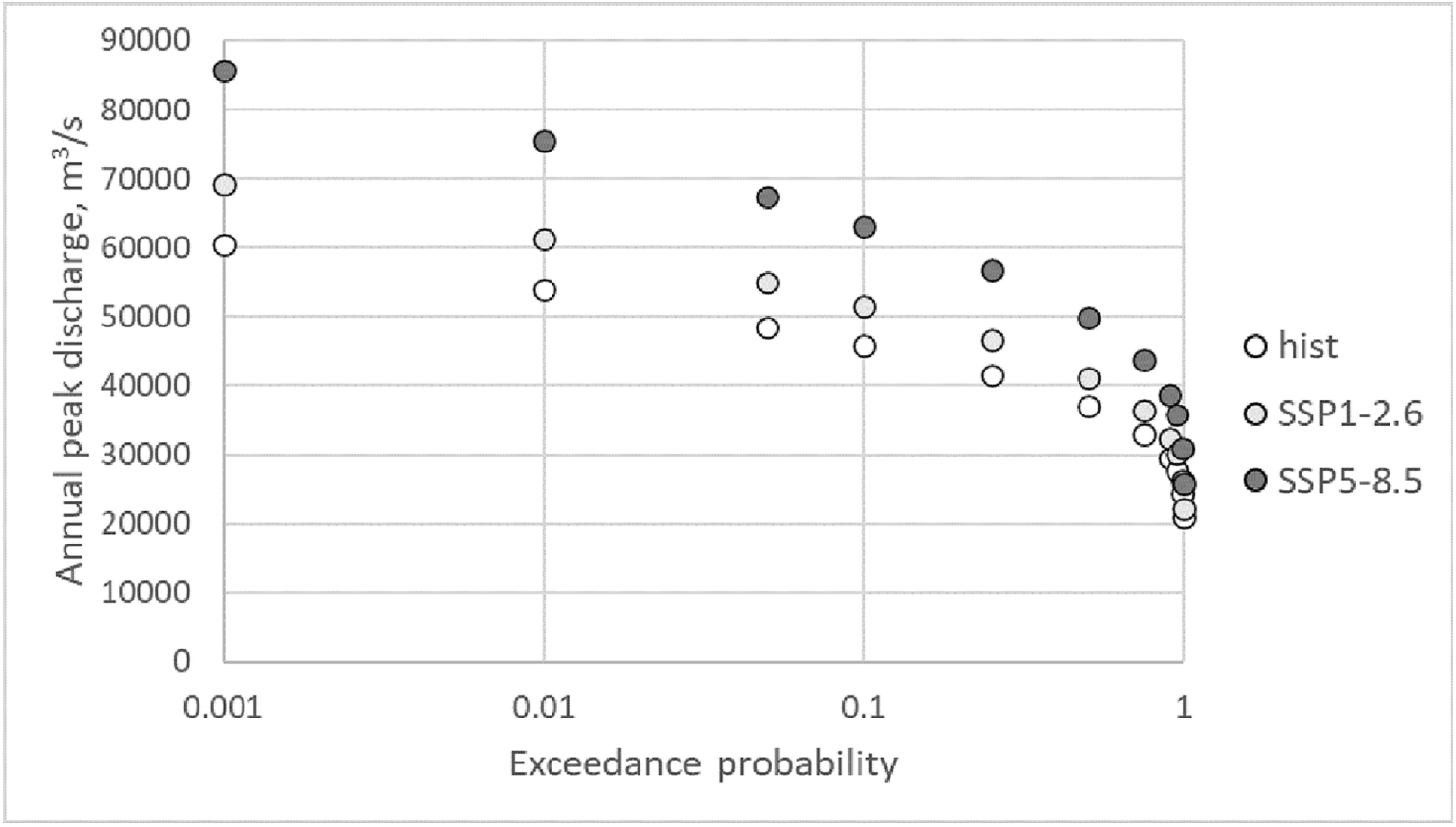


Figure 3

Exceedance probabilities of annual peak discharge simulated under different climate

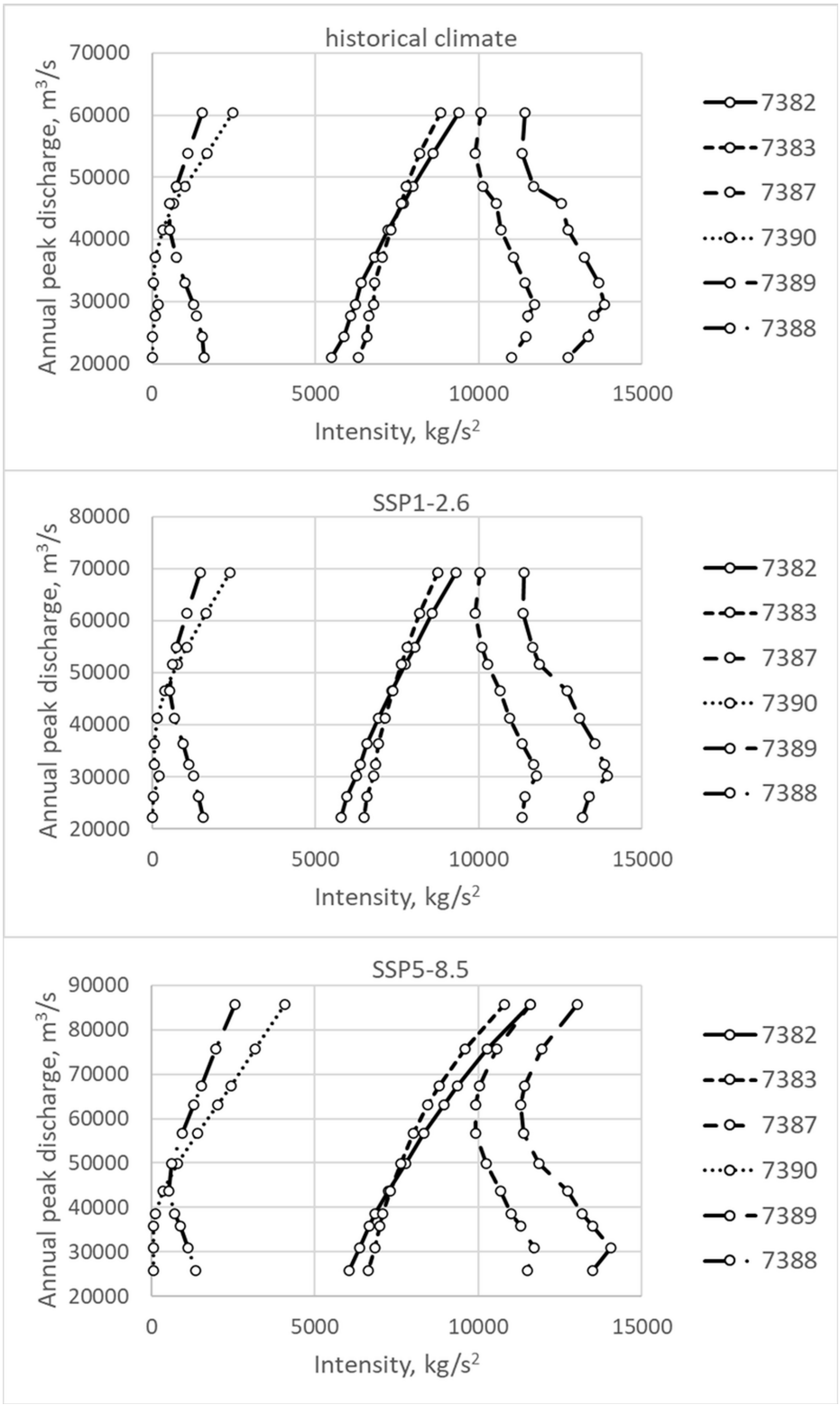


Figure 4

Q -1 relationships for some closely located model cells on the floodplain

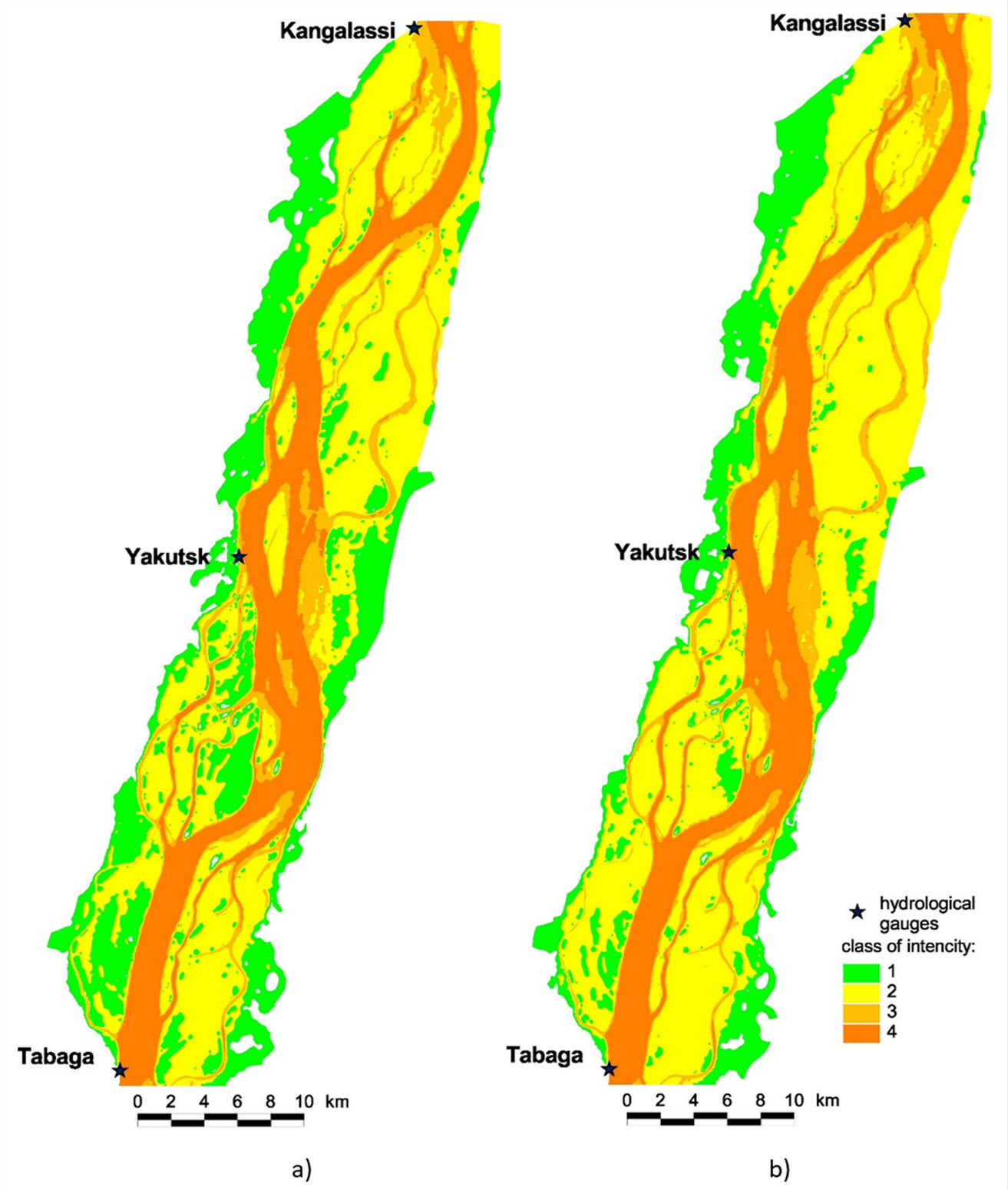


Figure 5

The damage indicators across the flood zone at a 1% probability inlet flow rate, corresponding to the current climate (a) and the SSP5-8.5 climate change scenario (b)

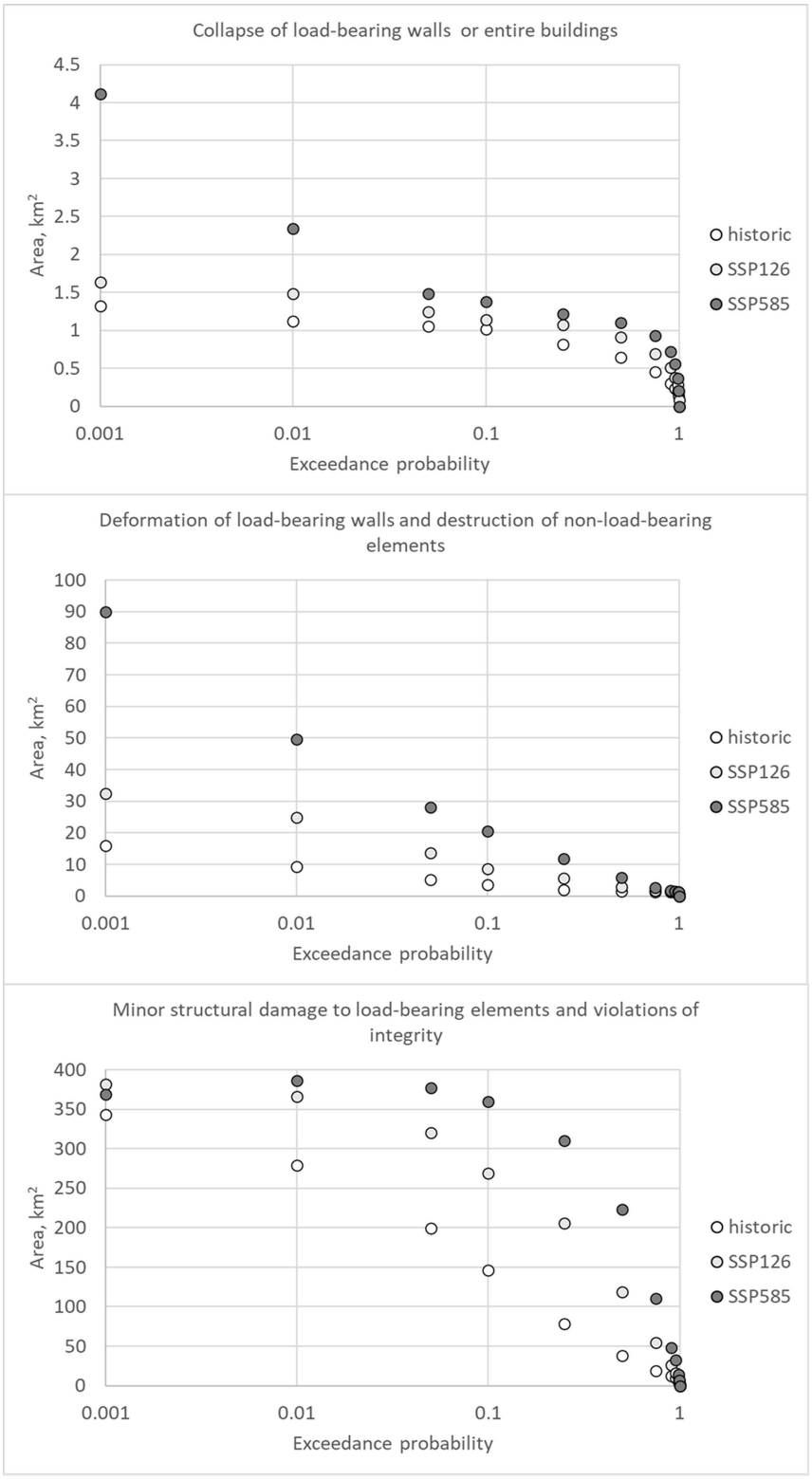


Figure 6

Exceedance probabilities of areas whose flooding would result in potential damage of varying levels under current and future climate conditions

Supplementary Files

This is a list of supplementary files associated with this preprint. Click to download.

- SupplementaryMaterial.docx